ACS Catalysis

Research Article

pubs.acs.org/acscatalysis

Oxygen Reduction on Graphene–Carbon Nanotube Composites Doped Sequentially with Nitrogen and Sulfur

Drew C. Higgins, Md Ariful Hoque, Fathy Hassan, Ja-Yeon Choi, Baejung Kim, and Zhongwei Chen*

Department of Chemical Engineering, Waterloo Institute for Nanotechnology, Waterloo Institute of Sustainable Energy, University of Waterloo, 200 University Avenue West, Waterloo, ON N2L 3G1, Canada

Supporting Information

ABSTRACT: The development of unique, reliable, and scalable synthesis strategies for producing heteroatom-doped nanostructured carbon materials with improved activity toward the electrochemical oxygen reduction reaction (ORR) occurring in metal–air batteries and fuel cells presents an intriguing technological challenge in the field of catalysis. Herein, we prepare unique graphene–carbon nanotube composites (GC) doped sequentially with both nitrogen and sulfur (GC-NLS) and subject them to extensive physicochemical characterization and electrochemical evaluation toward the ORR in an alkaline electrolyte. GC-NLS provides ORR onset potential increases of 50 and 70 mV in comparison to those of dual-doped individual graphene and carbon nanotubes, respectively. This highlights the significant synergistic effects that arise because of the nanocomposite arrangement, consisting of highly graphitized carbon nanotubes assembled on the surface of graphene sheets. The addition of sulfur as a co-dopant is also highly beneficial, providing an 80 mV increase in the ORR onset potential in comparison to that of GC nanocomposites doped with only nitrogen. Excellent electrochemical stability of GC-NLS is also observed through 5000 electrode potential cycles, indicating the promising potential of this new class of dual-doped GC nanocomposites as ORR catalysts.

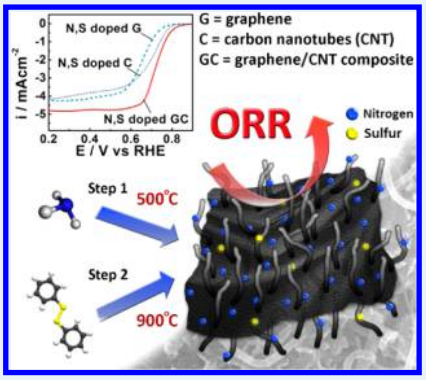

KEYWORDS: *electrocatalysis, oxygen reduction, nanocomposite, graphene, carbon nanotubes, metal–air batteries*

INTRODUCTION

Overcoming the inherently sluggish oxygen reduction reaction (ORR) kinetics is a primary technological challenge to improving the performance of fuel cells and metal–air batteries to practical levels.[1−3] To accomplish this, significant reliance on highly active platinum-based catalysts is maintained, despite the economic drawbacks, including excessive cost and monopolized supply. The development and validation of unique platinum-free electrocatalysts with high catalytic activity toward the ORR is a necessity and would perpetuate commercialization efforts for these clean operating and efficient electrochemical devices.

Nanostructured graphitic carbons such as graphene and carbon nanotubes (CNTs) have been the subject of intense research efforts recently because of their unique physical, chemical, and electronic properties. Numerous studies have focused on the development of innovative synthesis strategies for forming composites or fine-tuning the material properties, offering a portfolio of highly attractive functional materials for electrochemical applications such as batteries, fuel cells, and supercapacitors.[2,4−6] Graphene or CNTs particularly serve as suitable platforms for hosting highly active ORR surface moieties,[2,7,8] with increased turnover frequencies generally imparted by "doping" with heteroatoms such as nitrogen, boron, phosphorus, and sulfur.[9] Nitrogen-doped graphene (NG)[10−16] or CNTs (NCNTs)[17−23] have traditionally been the most extensively investigated, although practical synthesis strategies that can provide improved ORR activity are still required, albeit challenging. Recently, activity enhancements have been realized by the incorporation of a second heteroatomic dopant atom.[24−29] Additionally, combining heteroatom-doped graphene and CNTs into a nanocomposite arrangement has been demonstrated to be beneficial for ORR catalysis.[30−33] This is due to the synergistic contributions of each constituent, namely, the large surface areas and tunable surface chemistries of graphene,[4,34] and the interconnected and highly conductive three-dimensional architectures induced by the CNTs.[33] Despite the significant promise of these complementary configurations, only limited efforts have focused on the preparation and development of new graphene–CNT (GC) arrangements and have been confined to nitrogen doping.

In this study, we report the development of unique nitrogen- and sulfur-doped GC nanocomposites by a sequential doping process that provides enhanced activity and excellent stability toward the ORR in alkaline media. Adapted on the basis of a technique demonstrated to be beneficial to nitrogen- and boron-doped graphene catalysts,[26] the sequential doping process uses GC consisting of graphene oxide (GO) and CNTs. This preparation technique was selected to avoid complicated chemical vapor deposition processes and to

Received: March 22, 2014
Revised: June 13, 2014
Published: July 11, 2014

   dx.doi.org/10.1021/cs5003806 | ACS Catal. 2014, 4, 2734–2740

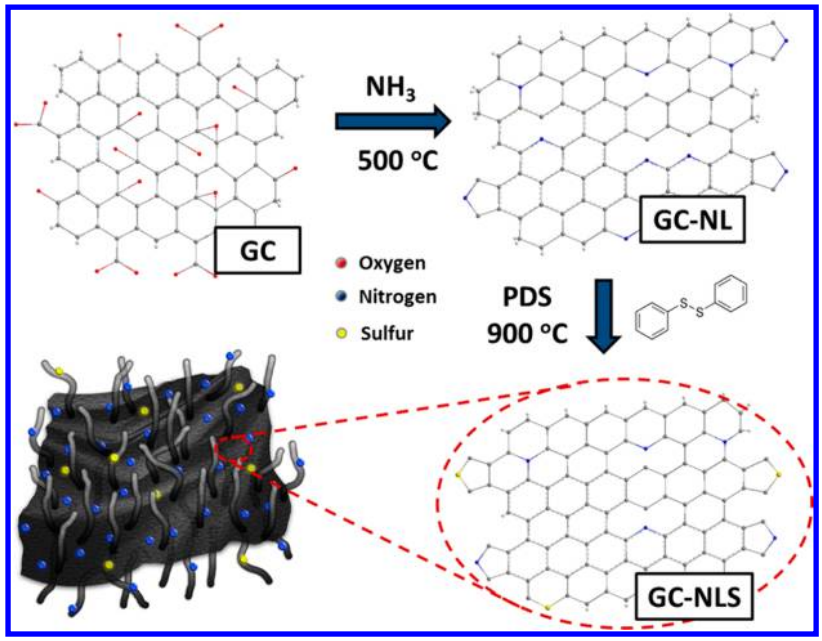

Figure 1. Schematic of the sequential doping process for preparing GC-NLS nanocomposites.

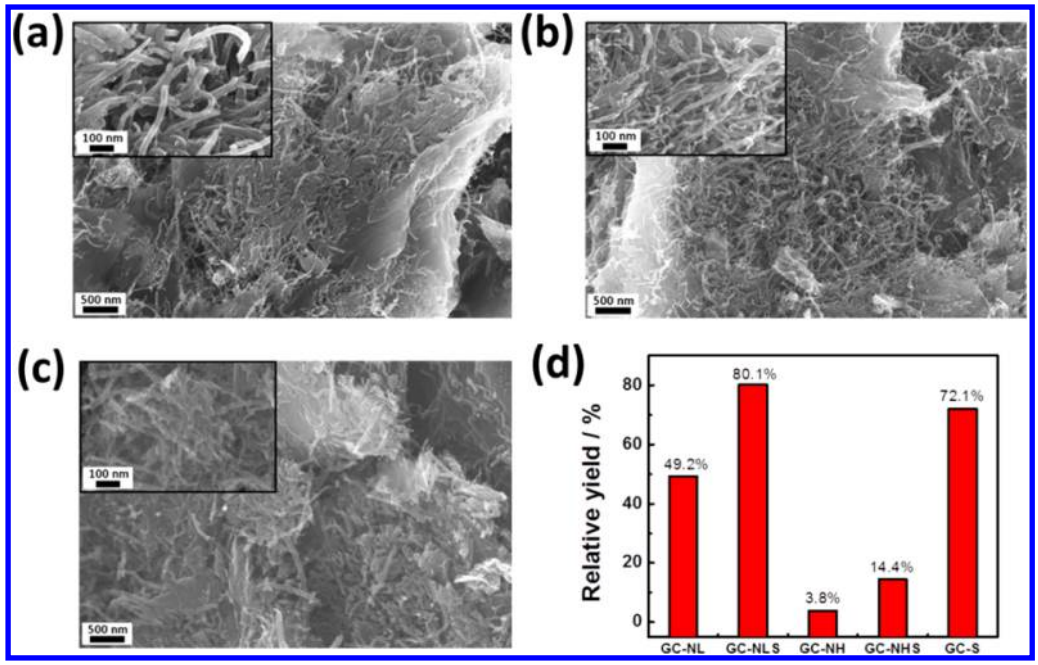

Figure 2. SEM images of (a) GC, (b) GC-NL, and (c) GC-NLS. (d) Yield of each step in the synthesis process.

circumvent the strong etching behavior,[35] incompatibility with co-dopants, and reduced nitrogen contents associated with high-temperature (700−1000 °C) ammonia treatments. The first step consists of a relatively low-temperature (500 °C) ammonia treatment for nitrogen doping of GC (GC-NL, L stands for low temperature), followed by mixing with phenyl disulfide (PDS) in a 1:5 (w/w) ratio (GC-NL to PDS) and heat treatment at 900 °C in argon for subsequent sulfur doping (GC-NLS). We exclusively demonstrate the beneficial ORR enhancements provided by this particular co-dopant arrangement, along with the advantageous nanocomposite configuration.

EXPERIMENTAL METHODS

Synthesis of the GC Nanocomposite. GO was prepared using an improved Hummers method reported previously.[8] Commercial CNTs were oxidized (O-CNTs) by being refluxed in 6 M nitric acid and subsequently washed.[36] GO and O-CNTs [5:1 (w/w)] were then physically mixed by sonication in acetone for 8 h while the water temperature in the sonicator was kept at ∼10 °C by the addition of ice. Acetone was then allowed to evaporate from the solution, and the graphene−carbon nanotube (GC) nanocomposites were collected for further processing.

Sequential Doping of GC-NLS. GC-NL was prepared by heating GC in a tube furnace at 5 °C min^{-1} to 500 °C, where it was held for 5 h under ammonia (60 sccm) and argon (140

dx.doi.org/10.1021/cs5003806 | ACS Catal. 2014, 4, 2734−2740

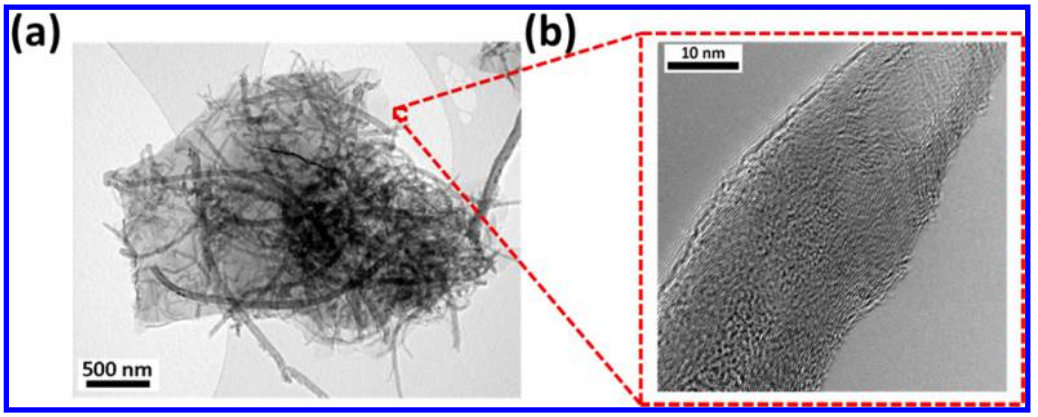

Figure 3. (a) TEM images of the GC-NLS showing the structure of intact graphene sheets with (b) highly graphitized CNTs assembled on the surface.

sccm) flows. The collected GC-NL was then physically ground with PDS [1:5 (w/w)] using a mortar and pestel and then pyrolyzed under pure argon at 900 °C for 5 h using the same heating rate that was used for the first step. For the purpose of comparison, a high-temperature (900 °C) initial ammonia treatment of GC was used to prepare GC-NH (where H stands for high-temperature treatment) and sequential sulfur doping (GC-NHS).

Synthesis of Comparison Materials. Several materials were prepared to provide comparison with the developed GC-NLS. First, GC-NL900 was prepared by heat treating GC-NL directly at 900 °C under argon. Nitrogen- and sulfur-doped graphene (G-NLS) and CNTs (C-NLS) were prepared by the same procedure that was used for GC-NLS, albeit using only individual GO and O-CNTs, respectively, as the starting materials. Sulfur-doped GC-S was prepared in the absence of any ammonia treatment by mixing GC and PDS in a 1:5 (w/w) ratio followed by pyrolysis under argon at 900 °C for 5 h. Finally, nitrogen- and boron-doped GC (GC-NLB) was prepared by a previously reported method,[26] which involves heat treating GC-NL with boric acid as the boron dopant source.

Electrochemical Characterization. Rotating disc electrode (RDE) testing was conducted to evaluate ORR activity. Four milligrams of catalyst was dispersed in 1 mL of an ethanol/DDI water [75:25 (v/v)] ink containing 0.05 wt % Nafion and 2 mg of Ketjenblack EC-600J carbon that helps to increase the level of dispersion of the catalyst in the ink and on the electrodes. Twenty microliters of the ink mixture was then deposited on a 0.19635 cm^2 electrode. Testing was conducted in 0.1 M KOH at room temperature and conducted by sweeping the electrode potential from 1.05 to 0.1 V versus the reversible hydrogen electrode (RHE) (10 mV s^{-1}) under oxygen saturation. Accelerated durability testing (ADT) was conducted by cycling the electrode potential 5000 times between 0.6 and 1.0 V vs RHE under nitrogen saturation.

RESULTS AND DISCUSSION

The overall sequential doping process for preparing GC-NLS nanocomposites sequentially doped with nitrogen and sulfur is illustrated in Figure 1. Minimal changes to the structure of GC (Figure 2a) are observed through scanning electron microscopy (SEM) after nitrogen doping (Figure 2b), and again after subsequent sulfur doping (Figure 2c). All samples display CNTs assembled on the surface of graphene, ideal for preventing sheet restacking during thermal reduction, and resulting in a well-integrated three-dimensional architecture.

A significant benefit of the fairly low-temperature (500 °C) ammonia treatment is highlighted by the yields of each individual synthesis step (Figure 2d), which was calculated taking into account only the GC-based precursors (i.e., the mass of the PDS precursor was omitted). More than 49% of the materials were recovered for GC-NL preparation, with the majority of the weight loss was attributed to the loss of oxygen species from GO during ammonia treatment.[37] Using 900 °C to dope GC-NH, however, resulted in a yield of only 3.8%, attributed to the powerful etching capabilities of ammonia at these elevated temperatures.[35] SEM imaging supports this claim (Figure S1 of the Supporting Information), whereby minimal graphene content remained and structural breakdown of some CNTs was observed. The morphological benefits of the GC-NLS were corroborated via transmission electron microscopy (TEM) imaging (Figure 3) that demonstrates intact graphene sheets with CNTs assembled on the surface, consistent with SEM results.

X-ray photoelectron spectroscopy (XPS) indicates successful nitrogen doping by ammonia treatment, with high-resolution N 1s spectra for GC-NL, GC-NLS, and GC-NH provided in panels a−c of Figure 4, respectively. Each signal was deconvoluted into four peaks arising from pyridinic-N (398.5 eV), pyrrolic-N (400.1 eV), graphitic-N (401.6 eV), and oxidized-N (405.1 eV) species.[21] GC-NL possesses a nitrogen surface concentration of 5.75 atom %, consistent with previous studies reporting nitrogen contents between ∼5.0 and 5.7 atom %, after treating GO by a similar process.[26,37] Conversely, the nitrogen content of GC-NH is reduced (3.71 atom %), consistent with the same reports indicating lower nitrogen contents at increasing temperatures.[26,37] After sulfur doping, the nitrogen content of GC-NLS drops significantly to 2.03 atom %, in agreement with the trend often observed with the addition of a second dopant atom.[24,26,38] The relative proportion of graphitic nitrogen in GC-NLS after nitrogen doping is also increased, highlighting the favorable existence of this species at elevated heat treatment temperatures.[37,39] Significant debate regarding the exact nitrogen species responsible for inducing ORR activity remains in the scientific literature.[16] While some reports attribute ORR activity to the presence of edge-plane-residing nitrogen moieties (i.e., pyridinic/pyrrolic),[40,41] others have linked ORR activity observations to increased graphitic nitrogen contents.[42,43] The increased relative graphitic content of GC-NLS may play

dx.doi.org/10.1021/cs5003806 | ACS Catal. 2014, 4, 2734−2740

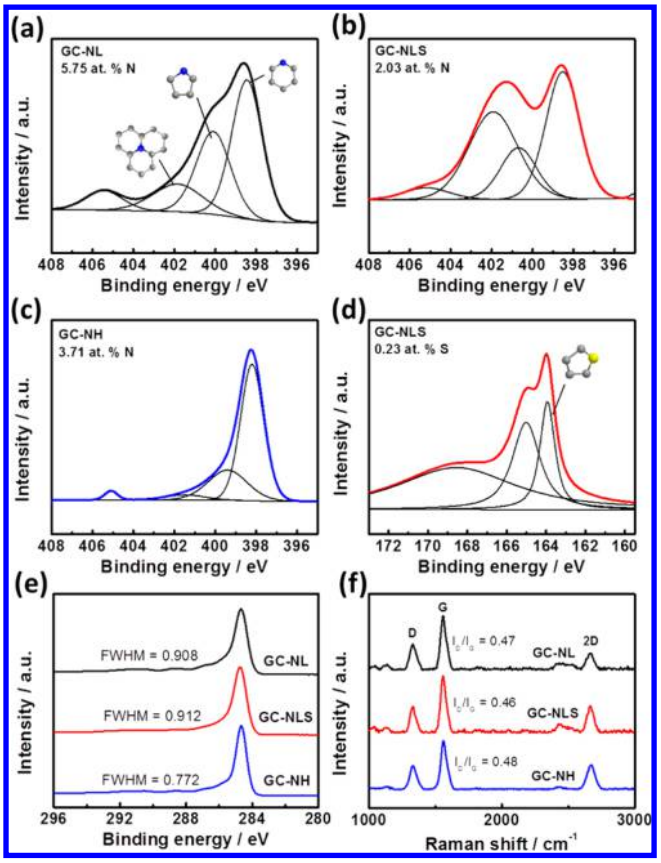

Figure 4. N 1s spectra of (a) GC-NL, (b) GC-NLS, and (c) GC-NH. (d) S 2p spectra of GC-NLS. (e) C 1s spectra and (f) Raman spectra of GC-NL, GC-NLS, and GC-NH.

a role influencing the ORR kinetics; however, further investigations are required in the scientific community to elucidate the exact role of various dopant species.

The incorporation of sulfur into GC-NLS is evidenced by the emergence of the S 2p doublet peaks located at 163.9 and 165.1 eV (Figure 4d). This indicates that sulfur resides primarily in the thiophenic arrangement,[24,44,45] with no clear presence of other sulfur species except for oxidized sulfur indicated by the peak at higher binding energies (~168.7 eV).[25,44] The sulfur content of GC-NLS is only ~0.23 atom %, a value lower than the sulfur content of 2.88 atom % reported by Liu et al.[29] for a templated nitrogen- and sulfur-doped carbon foam prepared using thiourea and glucose. This suggests that increased dopant contents can be obtained when heteroatom-containing precursors are used directly during nanostructured carbon formation. Additionally, the sulfur content of GC-NLS is significantly lower than the range of 1.30−1.53 atom % reported by Yang et al.[46] for GO heat-treated with benzyl disulfide. We attribute this to the fact that the incorporation of sulfur into structures such as partially or completely reduced graphene and CNTs is difficult,[38] particularly in comparison to that of GO with highly tunable surface functional species. This is supported by the results of GC-S preparation conducted by heat-treating (900 °C) a mixture of GC and PDS in argon directly that yields a sulfur content of 1.10 atom % (Figure S2 of the Supporting Information). Notwithstanding the relatively low sulfur content of GC-NLS, the synergistic effect toward the ORR is undeniable, as discussed below.

C 1s spectra obtained for GC-NL, GC-NLS, and GC-NH are displayed in Figure 4e, whereby the full widths at half-maximum (fwhms) are commonly used to quantify surface structural disorder.[47,48] The C 1s fwhm for GC-NL (0.908) increases only slightly after sulfur doping (0.912), indicating that in terms of surface disorder, the incorporation of a second adatom has a

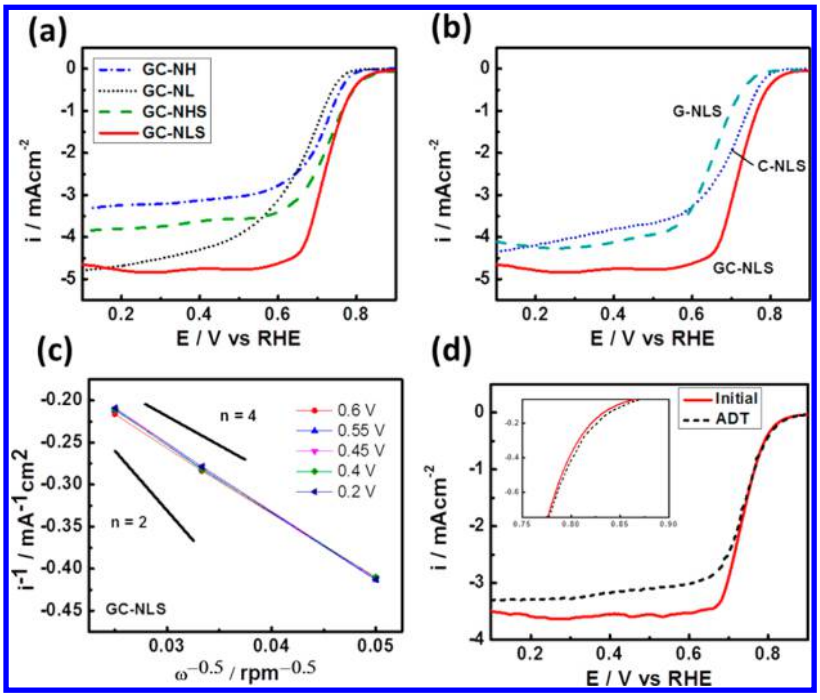

Figure 5. ORR activity of (a) GC-NH, GC-NL, GC-NHS, and GC-NLS in a 0.1 M KOH electrolyte with a 1600 rpm electrode rotation and 10 mV s^{-1} scan rate. (b) Evidence of the beneficial synergistic effect of GC-NLS in comparison to G-NLS and C-NLS. (c) Koutecky−Levich plots for GC-NLS at different electrode potentials. Calculated lines for n = 2 and n = 4 are shown for comparison. (d) ORR activity (900 rpm) before and after ADT consisting of 5000 cycles between 0.6 and 1.0 V vs RHE under nitrogen saturation.

dx.doi.org/10.1021/cs5003806 | ACS Catal. 2014, 4, 2734−2740

trade-off effect with the structural reorganization occurring at elevated temperatures. High-temperature ammonia-treated GC-NH demonstrates a lower C 1s fwhm (0.772) and a reduced level of surface disorder, in agreement with previously reported observations.[37] This is most likely due to an increased level of GO reduction at higher temperatures and preferential etching of ammonia toward disordered carbon species.[35]

Raman spectra of these graphitic materials (Figure 4f) display the characteristic D-band (1330 cm^{-1}), G-band (1560 cm^{-1}), and 2D-band (2667 cm^{-1}). Interestingly, the I_D/I_G band ratios used to gauge structural disorder[17] are virtually unchanged for all three materials and significantly lower than values commonly reported for doped graphene ($I_D/I_G > 1$).[10,11,24,26] This leads us to believe that the Raman signal arises primarily from the CNTs residing on the graphene surfaces, which still maintain their highly graphitic character through the stepwise doping process, as imaged through high-resolution TEM (Figure 3b).

ORR activities measured by RDE testing in 0.1 M KOH are displayed in Figure 5a and evaluated ORR kinetic parameters, including onset potentials (potential at which i = 0.1 mA cm^{-2}),[49] half-wave potentials ($E_{1/2}$), and diffusion-limited currents (i_L), summarized in Table 1. The beneficial impact

Table 1. ORR Kinetic Parameters for the Various Catalysts Investigated in This Study

catalyst	ORR onset potential (V vs RHE)[a]	$E_{1/2}$ (V vs RHE)	i_L[b]
GC-NH	0.79	0.71	−3.19
GC-NB	0.78	0.69	−4.38
GC-NL	0.77	0.66	−4.50
GC-NHS	0.85	0.72	−3.73
GC-NLS	0.85	0.72	−4.80
GC-S	0.58	0.49	−1.51
GC-NL900	0.81	0.67	−4.51
G-NLS	0.78	0.67	−4.22
C-NLS	0.80	0.69	−4.00

[a]Potential at which the ORR current density is 0.1 mA cm^{-2}. [b]Taken as the average of current densities from 0.2 to 0.4 V vs RHE.

of sulfur addition is apparent, whereby the onset potential and $E_{1/2}$ of GC-NLS increase by 80 and 60 mV, respectively, in comparison to those of GC-NL. A similar beneficial impact of sulfur doping is observed in the case of GC-NHS, exhibiting increasesin the onset potential and $E_{1/2}$ of 60 and 10 mV, respectively, relative to those of GC-NH. Notably, the fairly low-temperature ammonia treatment marks advantages in terms of electrochemical ORR performance. The ORR onset potential values on GC-NLS and GC-NHS are nearly identical (0.85 V vs RHE), suggesting similar active site structures in each catalyst; however, the current densities measured with GC-NLS in the mixed kinetic/mass transport limited region and at lower electrode potentials are significantly higher than those of GC-NHS. This highlights the fact that the low-temperature ammonia treatment serves to strike a balance among inherent ORR kinetics, active site densities, and catalyst morphology. Figure 5b also provides the ORR performance of GC-NLS in comparison to those of double-doped graphene (G-NLS) and CNTs (C-NLS) prepared by similar procedures, with SEM images and Raman spectra of these materials provided in Figures S3 and S4 of the Supporting Information, respectively. The ORR current density at GC-NLS is higher than that at G-NLS and C-NLS throughout the entire potential range investigated. The ORR onset potentials are 0.85, 0.80, and 0.78 V vs RHE, respectively, making readily apparent the benefits of the unique nanocomposite arrangement. This arrangement combines the ideal properties of graphene, including large surface areas and ease of functionalization,[4] with those of carbon nanotubes, including forming interconnecting networks and acting as spacers to prevent graphene sheet restacking.[33]

For GC-NLS, the increased mass transport limited current density in comparison to other materials investigated in this work indicates improved selectivity toward the efficient four-electron reduction of oxygen. Furthermore, the well-defined current density plateau at potentials below ∼0.6 V vs RHE indicates that the selectivity is not significantly changing as a function of electrode potential. Indeed, Koutecky−Levich plots of GC-NLS (Figure 5c) were prepared on the basis of polarization curves from various electrode rotation rates (Figure S5 of the Supporting Information) and were used to calculate the number of electrons transferred in the ORR to be between 3.6 and 3.8 over the range of potentials investigated. This indicates the consistent propensity of GC-NLS to preferentially reduce oxygen by the efficient four-electron process that has practical importance for metal−air battery and fuel cell performance. Furthermore, the stability of GC-NLS was investigated by accelerated degradation testing (ADT). After 5000 cycles between 0.6 and 1.0 V vs RHE, i_L was found to decrease slightly (Figure 5d), a commonly observed phenomenon thought to arise from electrode morphology changes.[50] The ORR kinetics are, however, not adversely affected (Figure 5d, inset), whereas commercial Pt/C (TKK, 15 μg of Pt cm^{-2}) displays a minor (∼15 mV) loss of onset and half-wave potential under identical conditions (Figure S6 of the Supporting Information). This indicates the excellent active site stability of GC-NLS under the potentiodynamic conditions of ADT.

As a 900 °C heat treatment was used for sulfur doping of GC-NLS, it is prudent to ensure that the beneficial ORR enhancements arose due to sulfur doping, and not from the structure- and surface-induced changes to GC-NL occurring at this elevated temperature. To accomplish this, as-prepared GC-NL was heat-treated at 900 °C in argon (GC-NL900). A slight increase in ORR activity (Figure S7 of the Supporting Information) is observed; however, the activity of GC-NL900 is still inferior to that of GC-NLS, highlighting the fact that sulfur indeed plays an important role in facilitating the ORR. While trace Mn residues from GO synthesis cannot be exclusively neglected, the significantly improved performance of GC-NLS in comparison to that the other materials prepared in this work, along with trace Mn-based catalysts reported recently,[51,52] provides an indication that activity enhancements primarily arise due to the synergistic GC composite arrangement and the sequential double doping procedure utilized. In terms of providing ORR activity, it has been suggested for NCNTs that the electronegativity of the nitrogen atoms induces a positive charge density on neighboring carbon atoms, enhancing oxygen adsorption and reactivity.[20] On the other hand, sulfur possesses an electronegativity very similar to that of carbon and thereby likely contributes to ORR activity in a very different way. Using computational simulations, Liang et al.[24] suggested that the interplay between the nitrogen and sulfur dopants leads to an increase in the spin and charge density of atoms present in graphene and by extension to an increase in ORR activity. Furthermore, it is expected that the presence of

dx.doi.org/10.1021/cs5003806 | ACS Catal. 2014, 4, 2734−2740

five-membered ring thiophenic sulfur results in an increased level of exposure of edge-plane carbon that has also been linked to ORR activity.[41,53] While both of these factors likely contribute to the ORR activity of GC-NLS, detailed computational simulations linked to surface sensitive probing techniques and electrochemical results are still necessary to elucidate the underlying mechanistic improvements.

Beyond the enhancements already presented, the sequential doping process of nitrogen and sulfur also provides other notable advantages. Attempts to simultaneously nitrogen and sulfur dope GC were largely unsuccessful, resulting in negligible product yields. Doping with only sulfur (GC-S) resulted in very limited ORR activity (Figure S8 of the Supporting Information). Also prepared were GC nanocomposites doped with nitrogen and boron (GC-NLB) in a stepwise fashion, as reported in the pioneering work of Zheng et al.[26] (Figure S9 of the Supporting Information). While the activity of these materials is improved relative to that of GC-NL, the ORR onset potential and $E_{1/2}$ are 70 and 30 mV lower on GC-NLB than on GC-NLS, respectively, highlighting the fact that sulfur is a more attractive co-dopant in this case.

CONCLUSIONS

In summary, we report the development of nitrogen- and sulfur-doped graphene−CNT nanocomposites prepared by a unique and scalable sequential doping process. Electrochemical evaluations revealed excellent electrochemical stability, along with significant ORR activity improvements linked to the incorporation of sulfur as a co-dopant, and synergistic enhancements provided by the nanocomposite arrangement. This paper therefore presents a new synthesis strategy for preparing double-doped nanostructured graphene−CNT composites with increased activity and electrochemical stability for the ORR, a process of practical importance in electrochemical energy technologies such as fuel cells and batteries.

ASSOCIATED CONTENT

Supporting Information

Detailed experimental information and nonessential materials characterization. This material is available free of charge via the Internet at http://pubs.acs.org.

AUTHOR INFORMATION

Corresponding Author

*E-mail: zhwchen@uwaterloo.ca. Phone: (519) 888-4567, ext. 38664.

Notes

The authors declare no competing financial interest.

ACKNOWLEDGMENTS

This work was supported by the University of Waterloo and the Waterloo Institute for Nanotechnology. TEM imaging was conducted at the Canadian Center for Electron Microscopy (CCEM) located at McMaster University (Hamilton, ON). This research was conducted as part of the Catalysis Research for Polymer Electrolyte Fuel Cells (CaRPE FC) Network administered from Simon Fraser University and supported by Automotive Partnership Canada (APC) Grant APCPJ 417858-11 through the Natural Sciences and Engineering Research Council of Canada (NSERC).

REFERENCES

(1) Chen, Z.; Higgins, D.; Yu, A.; Zhang, L.; Zhang, J. *Energy Environ. Sci.* **2011**, *4*, 3167−3192.
(2) Li, Q.; Cao, R.; Cho, J.; Wu, G. *Adv. Energy Mater.* **2014**, *4*, 1301415−1301434.
(3) Lee, D. U.; Choi, J.-Y.; Feng, K.; Park, H. W.; Chen, Z. *Adv. Energy Mater.* **2014**, *4*, 1301389−1301393.
(4) Chabot, V.; Higgins, D. C.; Yu, A.; Xiao, X.; Chen, Z.; Zhang, J. *Energy Environ. Sci.* **2014**, *7*, 1564−1596.
(5) Liang, Y.; Li, Y.; Wang, H.; Dai, H. *J. Am. Chem. Soc.* **2013**, *135*, 2013−2036.
(6) Xu, C.; Xu, B.; Gu, Y.; Xiong, Z.; Sun, J.; Zhao, X. S. *Energy Environ. Sci.* **2013**, *6*, 1388−1414.
(7) Jiang, Y.; Lu, Y.; Lv, X.; Han, D.; Zhang, Q.; Niu, L.; Chen, W. *ACS Catal.* **2013**, *3*, 1263−1271.
(8) Kim, B. J.; Lee, D. U.; Wu, J.; Higgins, D.; Yu, A.; Chen, Z. *J. Phys. Chem. C* **2013**, *117*, 26501−26508.
(9) Paraknowitsch, J. P.; Thomas, A. *Energy Environ. Sci.* **2013**, *6*, 2839−2855.
(10) Geng, D.; Chen, Y.; Chen, Y.; Li, Y.; Li, R.; Sun, X.; Ye, S.; Knights, S. *Energy Environ. Sci.* **2011**, *4*, 760−764.
(11) Higgins, D.; Chen, Z.; Lee, D. U.; Chen, Z. *J. Mater. Chem. A* **2013**, *1*, 2639−2645.
(12) Lee, D. U.; Park, H. W.; Higgins, D.; Nazar, L.; Chen, Z. *J. Electrochem. Soc.* **2013**, *160*, F910−F915.
(13) Lin, Z.; Waller, G.; Liu, Y.; Liu, M.; Wong, C.-P. *Adv. Energy Mater.* **2012**, *2*, 884−888.
(14) Qu, L.; Liu, Y.; Baek, J.-B.; Dai, L. *ACS Nano* **2010**, *4*, 1321−1326.
(15) Wu, G.; Mack, N. H.; Gao, W.; Ma, S.; Zhong, R.; Han, J.; Baldwin, J. K.; Zelenay, P. *ACS Nano* **2012**, *6*, 9764−9776.
(16) Wang, H.; Maiyalagan, T.; Wang, X. *ACS Catal.* **2012**, *2*, 781−794.
(17) Chen, Z.; Higgins, D.; Tao, H.; Hsu, R. S.; Chen, Z. *J. Phys. Chem. C* **2009**, *113*, 21008−21013.
(18) Chen, Z.; Yu, A.; Higgins, D.; Li, H.; Wang, H.; Chen, Z. *Nano Lett.* **2012**, *12*, 1946−1952.
(19) Gao, F.; Zhao, G.-L.; Yang, S. *ACS Catal.* **2014**, *4*, 1267−1273.
(20) Gong, K.; Du, F.; Xia, Z.; Durstock, M.; Dai, L. *Science* **2009**, *323*, 760−764.
(21) Higgins, D.; Chen, Z.; Chen, Z. *Electrochim. Acta* **2011**, *56*, 1570−1575.
(22) Higgins, D. C.; Wu, J.; Li, W.; Chen, Z. *Electrochim. Acta* **2012**, *59*, 8−13.
(23) Vazquez-Arenas, J.; Higgins, D.; Chen, Z.; Fowler, M.; Chen, Z. *J. Power Sources* **2012**, *205*, 215−221.
(24) Liang, J.; Jiao, Y.; Jaroniec, M.; Qiao, S. Z. *Angew. Chem., Int. Ed.* **2012**, *51*, 11496−11500.
(25) Xu, J.; Dong, G.; Jin, C.; Huang, M.; Guan, L. *ChemSusChem* **2013**, *6*, 493−499.
(26) Zheng, Y.; Jiao, Y.; Ge, L.; Jaroniec, M.; Qiao, S. Z. *Angew. Chem., Int. Ed.* **2013**, *125*, 3192−3198.
(27) Su, Y.; Zhang, Y.; Zhuang, X.; Li, S.; Wu, D.; Zhang, F.; Feng, X. *Carbon* **2013**, *62*, 296−301.
(28) Chung, H. T.; Johnston, C. M.; Artyushkova, K.; Ferrandon, M.; Myers, D. J.; Zelenay, P. *Electrochem. Commun.* **2010**, *12*, 1792−1795.
(29) Liu, Z.; Nie, H.; Yang, Z.; Zhang, J.; Jin, Z.; Lu, Y.; Xiao, Z.; Huang, S. *Nanoscale* **2013**, *5*, 3283−3288.
(30) Chen, P.; Xiao, T.-Y.; Qian, Y.-H.; Li, S.-S.; Yu, S.-H. *Adv. Mater.* **2013**, *25*, 3192−3196.
(31) Park, H. W.; Lee, D. U.; Liu, Y.; Wu, J.; Nazar, L. F.; Chen, Z. *J. Electrochem. Soc.* **2013**, *160*, A2244−A2250.
(32) Tian, G.-L.; Zhao, M.-Q.; Yu, D.; Kong, X.-Y.; Huang, J.-Q.; Zhang, Q.; Wei, F. *Small* **2014**, *10*, 2251−2259.
(33) Ratso, S.; Kruusenberg, I.; Vikkisk, M.; Joost, U.; Shulga, E.; Kink, I.; Kallio, T.; Tammeveski, K. *Carbon* **2014**, *73*, 361−370.
(34) Allen, M.; Tung, V.; Kaner, B. *Chem. Rev.* **2010**, *110*, 132−145.
(35) Jaouen, F.; Dodelet, J.-P. *J. Phys. Chem. C* **2007**, *111*, 5963−5970.

(36) Higgins, D. C.; Choi, J.-Y.; Wu, J.; Lopez, A.; Chen, Z. *J. Mater. Chem.* **2012**, *22*, 3727−3732.
(37) Li, X.; Wang, H.; Robinson, J. T.; Sanchez, H.; Diankov, G.; Dai, H. *J. Am. Chem. Soc.* **2009**, *131*, 15939−15944.
(38) Shi, Q.; Peng, F.; Liao, S.; Wang, H.; Yu, H.; Liu, Z.; Zhang, B.; Su, D. *J. Mater. Chem. A* **2013**, *1*, 14853−14857.
(39) Liu, R.; Wu, D.; Feng, X.; Müllen, K. *Angew. Chem., Int. Ed.* **2010**, *122*, 2619−2623.
(40) Maldonado, S.; Stevenson, K. J. *J. Phys. Chem. B* **2005**, *109*, 4707−4716.
(41) Matter, P. H.; Zhang, L.; Ozkan, U. S. *J. Catal.* **2006**, *239*, 83−96.
(42) Lai, L.; Potts, J. R.; Zhan, D.; Wang, L.; Poh, C. K.; Tang, C.; Gong, H.; Shen, Z.; Lin, J.; Ruoff, R. S. *Energy Environ. Sci.* **2012**, *5*, 7936−7942.
(43) Niwa, H.; Horiba, K.; Harada, Y.; Oshima, M.; Ikeda, T.; Terakura, K.; Ozaki, J.-i.; Miyata, S. *J. Power Sources* **2009**, *187*, 93−97.
(44) Yang, S.; Zhi, L.; Tang, K.; Feng, X.; Maier, J.; Müllen, K. *Adv. Funct. Mater.* **2012**, *22*, 3634−3640.
(45) Higgins, D.; Hoque, M. A.; Seo, M. H.; Wang, R.; Hassan, F.; Choi, J.-Y.; Pritzker, M.; Yu, A.; Zhang, J.; Chen, Z. *Adv. Funct. Mater.* **2014**, *24*, 4325−4336.
(46) Yang, Z.; Yao, Z.; Li, G.; Fang, G.; Nie, H.; Liu, Z.; Zhou, X.; Chen, X.; Huang, S. *ACS Nano* **2012**, *6*, 205−211.
(47) Maldonado, S.; Morin, S.; Stevenson, K. J. *Carbon* **2006**, *44*, 1429−1437.
(48) Ramaswamy, N.; Tylus, U.; Jia, Q.; Mukerjee, S. *J. Am. Chem. Soc.* **2013**, *135*, 15443−15449.
(49) Wu, G.; More, K. L.; Johnston, C. M.; Zelenay, P. *Science* **2011**, *332*, 443−447.
(50) Wu, G.; Nelson, M. A.; Mack, N. H.; Ma, S.; Sekhar, P.; Garzon, F. H.; Zelenay, P. *Chem. Commun.* **2010**, *46*, 7489−7491.
(51) Masa, J.; Zhao, A.; Xia, W.; Muhler, M.; Schuhmann, W. *Electrochim. Acta* **2014**, *128*, 271−278.
(52) Masa, J.; Zhao, A.; Xia, W.; Sun, Z.; Mei, B.; Muhler, M.; Schuhmann, W. *Electrochem. Commun.* **2013**, *34*, 113−116.
(53) Chen, Z.; Higgins, D.; Chen, Z. *Electrochim. Acta* **2010**, *55*, 4799−4804.